A Low-Cost Ultra Low Profile Phased Array System for Mobile Satellite Reception Using Zero-Knowledge Beamforming Algorithm

Pedram Mousavi, *Member, IEEE*, Mohammad Fakharzadeh, S. Hamidreza Jamali, Kiarash Narimani, Mircea Hossu, Hamid Bolandhemmat, Gholamreza Rafi, and Safieddin Safavi-Naeini, *Member, IEEE*

***Abstract*—In this paper, a stair-planar phased array antenna system for mobile broadcast satellite reception in Ku-band will be introduced. The height of the antenna is only 6 cm and the system has two-dimensional electronic scanning capability. The design procedures of low profile high gain microstrip sub-array antennas, low noise amplifiers, hybrid analog phase shifters, along with a novel fast electronic beamforming algorithm will be discussed in this paper. The mobile phased array antenna receives LHCP and RHCP signals simultaneously. For each polarization 496 microstrip elements have been used to provide a radiation gain of 31.5 dBi. This phased array system scans $\pm 2.8^\circ$ in azimuth and $\pm 20^\circ$ in elevation with less than 3 dB scanning loss. The main objective of this design is to develop a Ku-band phased array system with very low cost components and a minimum number of tracking sensors. A novel beamforming algorithm compensates for the fabrication inaccuracies of the microwave components and variations in their characteristics due to ambient changes. Neither *a priori* knowledge of the satellite's direction, nor the phase-voltage characteristic of the phase shifters are required in this algorithm which results in eliminating an expensive laborious calibration procedure. The real time field tests verify that the developed mobile antenna system can nullify the base vehicle yaw disturbances up to 60 deg/s and 85 deg/s^2.**

***Index Terms*—Beamforming, mobile reception, phased array antenna, satellite antenna, satellite communications system, tracking system.**

I. Introduction

DURING THE past two decades, there has been an increasing demand for mobile satellite broadcasting and communications especially in vehicular stations [1]–[7]. Vehicle mounted antennas are one of the most critical parts in providing the satellite services for moving vehicles. Beside of satisfying the basic requirements such as high radiation gain, the vehicle mounted antenna should be capable of satellite tracking for fast moving conditions. Cars on the roads are not only moving forward, but changing lanes, going over bumps, and turning corners and all such motions must be compensated for by the antenna tracking system so that antenna can maintain the received satellite signal above the desired level.

Reflector antennas with rather high gain are necessary for reasonable signal reception quality for Ku-band satellite communications. However, they cannot be used on small to midsize vehicles such as SUVs and minivans because of restriction on dimensions and aerodynamics. Instead, relatively flat antennas are desirable for this type of applications.

Several issues need to be addressed in designing a low profile antenna for commercial applications. The system must be extremely low profile even below 10 cm in order to satisfy the aerodynamic requirements of the vehicles. One of the challenges in reducing the height especially if the system requires to work in a wide geographic region such as the continental United States and Canada with the EIRP of 53 dBW is to maintain a sufficient gain over a relative wide range of elevation angles, i.e., from 20° to 70°. Experiments have shown that the medium-size cars may turn as fast as 60 deg/s with an angular acceleration of up to 100 deg/s^2. Having considered the narrow beam width in azimuth, this is a serious challenge for any mobile antenna system. Another important issue is the cost of the mobile antenna system for commercial application. The cost includes expensive antenna and microwave components to sustain the high gain; high precision sensors such as gyro, tilt sensor and GPS and also costly mechanical platform. Currently two low profile antennas are available in the market [3], [4]; and also several designs can be found in the literatures [5]–[7].

In [3] the antenna array consists of a whole planar array structure with the stacked microstrip antenna fed by a waveguide feed network. This complicated waveguide feed network increases the production cost. The size of array is limited in order to keep the feed loss minimum, therefore the achieved gain is not sufficient to maintain the required signal level in various weather conditions. Whole planar array structure limits the elevation coverage of the antenna since it requires to be tilted mechanically to the direction of the satellite and at the same time the array needs to be confined in the restricted profile of the system (13.5 cm in height).

The mechanical tracking unit needs to compensate for all the car movements including all the tiny bumps on the road which

Manuscript received March 11, 2008; revised June 11, 2008. Current version published December 30, 2008. This work was supported in part by Intelwaves Technologies Ltd., the Ontario Centre of Excellence (OEC), the National Science and Engineering Research Council of Canada (NSERC), and in part by Research In Motion (RIM).

P. Mousavi, M. Fakharzadeh, S. H. Jamali, K. Narimani, M. Hossu, H. Bolandhemmat, and G. Rafi are with Intelwaves Technologies Ltd., Waterloo, ON N2L 6J2, Canada (e-mail: Pmousavi@intelwaves.com).

M. Fakharzadeh, S. H. Jamali, S. Safavi-Naeini, and H. Bolandhemmat are with the Electrical and Computer Engineering Department, University of Waterloo, Waterloo, ON N2L 3G1, Canada.

S. H. Jamali is with the Electrical and Computer Engineering Department, University of Tehran, Tehran 14155, Iran (e-mail: jamali@maxwell.uwaterloo.ca).

Color versions of one or more of the figures in this paper are available online at http://ieeexplore.ieee.org.

Digital Object Identifier 10.1109/TAP.2008.2005928

generate weak disturbance in elevation. Considering the mechanical nature of its tracking system, constant movement of the servo translates into susceptibility to noise, and unreliability. The lack of agility stemming from the antenna inertia and its excessive weight, therefore, limits how fast a car could maneuver not to lose the signal. This bounds the angular velocity such that vehicle can turn with a maximum rate of 30 deg/s.

The stair-planar array is utilized in [4] to increase the elevation coverage range of the mobile antenna system. The array scans mechanically in both azimuth and elevation plane. The antenna arrangements form a spatial phased array is able to track a satellite in an elevation plane by mechanically rotating the antenna panels about transverse axes. This gives rise to generation of respective elevation angles and changing the respective distances between the axes. However, the antenna requires an extra servo motor to change the distance between each panel. Also the antenna generates a relatively narrow azimuth beam width which makes it difficult to compensate the car movement in azimuth. Therefore, the tracking speed in azimuth is less than 30 deg/s.

In [5] a flat waveguide slot array with wide beam in elevation was used. Therefore, the mechanical tracking is only in azimuth plane. The gain of this configuration is low (26.5 dBi) and it has limited elevation coverage. In [6] a stair-planar configuration was used. This system uses a one-dimensional electronic beam scanning in elevation and mechanical scanning in azimuth. During satellite tracking, the system is operated by the squinted beam tracking with respect to the main beam. Two-level phase-shifters are used to make the main beam as well as the squint beam. The squint beam technique requires complex and expensive extra phase shifters and also a time consuming calibration procedure.

In [7] a compact offset reflector for broadband and direct broadcast services in Ka/K-band and Ku-band was developed. Similar squint beam scanning scheme implemented in Ku-band using 2×2 array in the feed of the reflector antenna. This system requires several tracking sensors including magnetic compass, tilt sensor, gyro, and GPS. The data presented demonstrates that system can compensate for a weak disturbance in roll, pitch and yaw.

In this paper we consider the use of stair-planar phased array antenna with electronic beamforming in both azimuth and elevation planes. Contrary to whole planar array structure and compact offset reflector, the stair-planar structure has the advantage of being low profile. In our design the height of the system is less than 6 cm including the radome, which according to the authors' best knowledge is the lowest profile commercially available antenna for mobile direct broadcasting satellite (DBS) application. This structure is optimized to have a minimum number of phase shifters and active channels (17 for each polarization) while maintaining the scanning capability and the required gain.

However, utilizing phased array antenna in commercial applications has many serious tracking challenges to deal with. By reducing the height; in order to maintain enough antenna gain one needs to increase the diameter of the system. Therefore, a fan beam is formed which is very narrow in azimuth and relatively wide in elevation, which makes it extremely difficult to sustain the beam aimed to the satellite.

Another challenge is the electronic beamforming as an essential part of the control loop in both homing and tracking modes. To implement this technique a prior knowledge of the phase-voltage characteristics of the phase shifters is required. As these characteristics are device dependent and they may change with the environmental conditions, like temperature and humidity, as well as aging, a non-model based algorithm for the beamforming is required [8].

To achieve this crucial requirement, an innovative beamforming technique is devised which does not require the knowledge of system model parameters in general. This technique is referred to as the zero-knowledge beamforming. Utilizing this new beamforming techniques not only reduces the cost of the microwave devices such as phase shifter, but also reduces the number of tracking sensors such as Gyro and GPS and provides the opportunity to use less expensive sensors.

The rest of the paper is organized as follows. In Section II we describe the array system configuration and briefly discuss the G/T requirements. In Section III, we explain the components of the phased array system such as microstrip sub-array antenna, LNA and phase shifter. Section IV is devoted to describing a novel tracking algorithm based on zero-knowledge beamforming. The experimental results are presented in Section V. Finally Section VI concludes the paper.

II. System Configuration

In this section the general system configuration is discussed. This includes the total array gain and the method of optimizing the number of active channels to achieve the required G/T.

A. General System Configurations

Fig. 1 shows the configuration and block-diagram of the proposed system. The antenna system is a phased array antenna with stair-planar configuration. The system composed of ten rows with each row including three to four radiating modules in the form of 2×8 and 2×16 microstrip sub-arrays, which form a non-uniform array. The first front five rows support left hand circular polarization (LHCP) and the back five rows support the right hand circular polarization (RHCP). There are 17 sub-arrays for each polarization. Three of them are 2×8 and the rest are 2×16 which in total 496 microstrip elements are used for each polarization. The sub-arrays are mounted on array carriers which can mechanically rotate from 20° to 70° in elevation plane. The sub-arrays are connected to the low noise amplifier (LNA) and through the corresponding cable to the phase shifter/power combiner (PS/PC) box. The phase of the received signal by each sub-array is controlled by an analog phase shifter and combined with the signals of the other sub-arrays of the same polarization. The combined signal is amplified and then down-converted by a low noise block (LNB). The down-converted signal is further processed by the DVB board for extraction of the satellite ID and is sent to the receiver inside the car through a Rotary Joint. The RF detector implemented in the DVB board further measures the strength of the signal. The hardware boards include main Control Board and several auxiliary boards such as digital to analog converter to control the voltage of the phase shifters, gyro board, motor control and

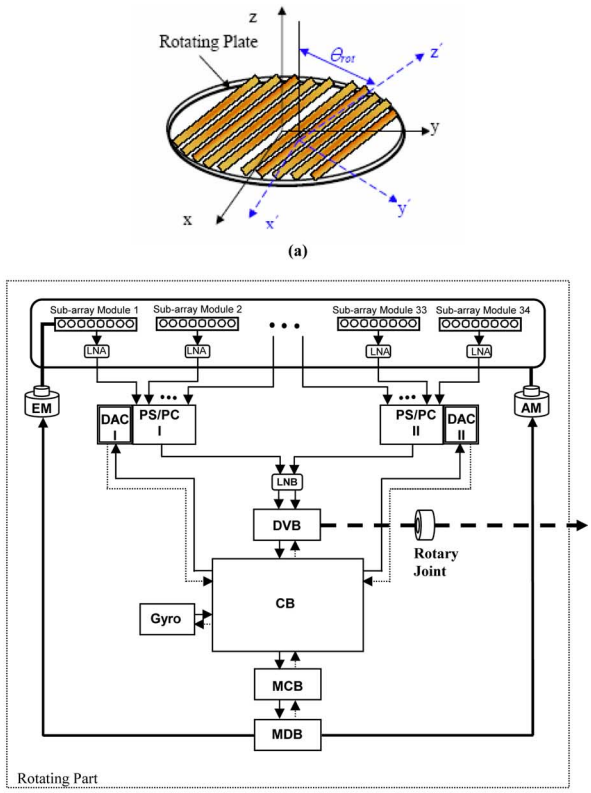

Fig. 1. Block diagram of the stair phased array antenna system. (a) Phased array antenna. (b) System configuration.

TABLE I
LOW PROFILE SYSTEM PARAMETERS

Parameters	Value
Frequency	12.2-12.7 GHz
Polarization	Dual Circular
Gain	31.5 dB (per polarization)
Axial ratio	<1.8 dB
Tracking speed (Azimuth)	60°/sec
Spatial coverage	0°-360° Azimuth 20°-70° Elevation
System height	6 cm
System diameter	86 cm
System weight	12 Kg

driver boards. A compact and light mechanical platform is designed for the phased array system. The mechanical system is comprised of rotating and stationary parts. The stationary part is attached to the roof of the vehicle with roof bars. All above mentioned electronic parts are integrated in the rotating part. The details of the mechanical system are beyond the scope of this publication and deserve a separate treatment. The overall system design parameters are summarized in Table I.

TABLE II
COMPONENTS PARAMETERS

Parameter	Value	Comment
LNA gain	23 dB	Minimum gain
LNA noise figure	0.8 dB	Maximum NF
Cable loss	1.5 dB	Cable and connector losses
PSPC loss	5~7 dB	2 dB loss variation
2x16 sub-arrays directivity	21.8 dB	
Feed network loss	1.3 dB	
Sky temperature T_i	40°~85 °K	
Ground temperature T_0	290 °K	Typical
Wavelength λ	24 mm	Ku band frequency

B. Total Array Gain and Radiation Pattern

Total array gain combines the radiation gain of all antenna elements. For uniform arrays, where all elements are identical, the total array gain is equal to the product of the element gain and the array factor. Since the array shown in Fig. 1(a) is a non-uniform array, the expression for the total array gain, $G(\theta, \phi)$, is more complex than a uniform array. With some simplifications, we can show that the total radiation gain of this array for each polarization is given by

$$G(\theta,\varphi) = \sum_{m=1}^{17} w_m^* [\alpha(m) g_{2\times 16}(\theta',\varphi') + \beta(m) g_{2\times 8}(\theta',\varphi')] \exp(jk_0 \mathrm{r}\cdot \mathrm{R_m}) \quad (1)$$

where w_m^* is the weight of phase shifter $m, \alpha(m)$ is 1 for 2×16 elements and 0 for 2×8 elements,$\beta(m)$ is 1 for 2×8 elements and 0 for 2×16 elements. Also $g_{2\times 8}(\theta',\varphi')$ and $g_{2\times 16}(\theta',\varphi')$ are the spherical radiation patterns of 2×8 and 2×16 sub-arrays in their own coordinates system which will be discussed shortly. Moreover, k_0 is the wave constant ($k_0 = 83\pi$ at 12.45 GHz), $\mathbf{r} = [\sin\theta_{\mathrm{sat}}\cos\varphi_{\mathrm{sat}} \;\; \sin\theta_{\mathrm{sat}}\sin\varphi_{\mathrm{sat}} \;\; \cos\theta_{\mathrm{sat}}]$ shows the satellite direction, and $\mathbf{R_m} = [x_m \;\; y_m \;\; z_m]$ denotes the coordinates of element m in the array reference system.

Considering ideal phase shifters and assuming the maximum radiation gains of 2×8 and 2×16 elements are respectively 17.9 dBi and 20.2 dBi (Section III.A), one can show that the minimum ideal array gain is 32.17 dBi. Considering the insertion loss of the feed network it can be shown that the actual gain of the phase array is reduced to 31.5 dBi [9]. The 2D radiation pattern of the whole array will be demonstrated later (in Section V). Since sub-arrays can rotate in elevation and azimuth, we have to define two coordinates systems to find the 3D radiation pattern of the whole array antenna, as shown in Fig. 1(a).

1- Array coordinates system, which is used to find the inter-element phase-lags and adjust the phase shifter weights is denoted by (x, y, z).
2- Sub-array coordinates system which is a rotating coordinates system used to find the radiation gain of sub-arrays (elements), denoted by (x', y', z').

In Fig. 1(a) θ_{rot} denotes the rotation of the sub-array's normal vector in elevation direction. The sub-array's rotation in azimuth is not important because the array and elements rotate together and we can always assume that both coordinates systems share

TABLE III
POSITION OF SUB-ARRAYS IN PHASED ARRAY ANTENNA CONFIGURATION

Polarization	1st Row		2nd Row		3rd Row		4th Row		5th Row	
	Number of sub-arrays	sub-array configuration	Number of sub-arrays	sub-array configuration	Number of sub-arrays	sub-array configuration	Number of sub-arrays	sub-array configuration	Number of sub-arrays	sub-array configuration
LHCP	1 2	**2x8** **2x16**	3	**2x16**	3	**2x16**	1 3	**2x8** **2x16**	1 3	**2x8** **2x16**
RHCP	1 3	**2x8** **2x16**	1 3	**2x8** **2x16**	3	**2x16**	3	**2x16**	1 2	**2x8** **2x16**

the same x-axis. For a target located at (θ, ϕ) in the array coordinates system, the transferred coordinates in the sub-array coordinates system (θ', ϕ'), can be found from the following:

$$\begin{cases} x = \sin(\theta)\cos(\varphi) \\ y = \sin(\theta)\sin(\varphi) \\ z = \cos(\theta) \end{cases} \tag{2-a}$$

$$\begin{cases} x' = x \\ y' = y\cos(\theta_{\rm rot}) + z\sin(\theta_{\rm rot}) \\ z' = -y\sin(\theta_{\rm rot}) + z\cos(\theta_{\rm rot}) \end{cases} \tag{2-b}$$

$$\begin{cases} r' = \sqrt{x'^2 + y'^2} \\ \varphi' = \cos^{-1}\left[\frac{x'}{r'}\right] \\ \theta' = \tan^{-1}\left[\frac{r'}{z'}\right]. \end{cases} \tag{2-c}$$

Hence, the maximum received signal is obtained when the satellite is along the z'-axis and phased shifters are adjusted to compensate the inter-element phase-lags completely.

C. G/T Calculation

The required average G/T for mobile antenna system in North America is approximately 9.5–10 dB/°K with EIRP of 53 dBW. The number is basically the compromise between the performances of the antenna in various environmental conditions such as rain and snow and the acceptable profile for vehicular application. To evaluate the performance and the development cost of the phased array, one has to estimate how many active channels are needed to meet the above stated G/T requirement. Assuming the losses of all RF channels are identical except for the loss of the phase shifter the overall G/T of the system can be calculated as [10]

$$\frac{G}{T} = \frac{NG_e\eta}{T_i + T_0\left(L_fF - 1 - \frac{L_f}{g} + \frac{N}{\sum_{k=1}^{N} 1/L_k} \times \frac{L_f}{g} \times L_d\right)} \tag{3}$$

where g and F are the gain and noise figure of the LNA, L_f and L_d are the sub-array feed-network loss and cable loss which are assumed to be identical for all channels, L_k is the kth PS/PC individual channel loss. G_e is the effective directivity of each antenna sub-array and η is the aperture efficiency. Also T_o and T_i are the room, and the sky temperatures, respectively. The typical components parameters are summarized in Table II.

To meet the 9.5–10 dB/°K dB requirement for the above value, the number of 2×16 sub-arrays should be more than 15 sub-arrays. As mentioned above for each polarization 17 sub-arrays of different sizes were used, which are equivalent to 15.5 2×16 sub-arrays. The combination of sub-arrays for each row of Fig. 1 is summarized in Table III.

III. KU-BAND COMPONENTS

In this section the design procedures of the major Ku-band microwave components used for this system, are described. These components are the microstrip sub-array antenna and the corresponding feed network, LNA, and the analog phase shifter.

A. Sub-Array Antenna and Feed-Network

The challenges arising from the development of the Ku-band sub-array antenna include the minimization of the sub-array's feed-network loss, the attainment of the required 4% bandwidth and at the same time reducing the width of the sub-arrays which directly affect the overall height of the system. In this application microstrip antenna sub-array is used due to its ease of manufacturing, low cost, low profile, and light weight. The circular polarization is achieved by employing the sequential rotation technique [11] in which each patch is excited at a single feed point. The elements of the sub-array are fed by a corporate microstrip feed network to keep the overall constructional complexity at the minimum and maintain a compact size. Three major steps are required to develop a high gain sub-array antenna [12]:

- The single patch element development (in this work a square patch with two truncated corners is used [12]);
- The building block sub-array development to maintain the acceptable axial ratio (AR) over the band of operation;
- The full sub-array development.

Fig. 2(a) depicts the top and the side-view of a single array element. The substrate of the array elements is constituted of a top layer of Rogers RT 5880 with dielectric constant of ε_r= 2.2 and the loss tangent of 0.0009 at 10 GHz and a bottom layer of RO3003 with dielectric constant of $\varepsilon_r = 3.0$ and the loss tangent of 0.0013 at 10 GHz. To achieve a wider bandwidth and higher gain, the top substrate thickness is set to 1.57 mm (0.0625λ). The feed-network is constructed on the lower substrate with thickness of 0.5 mm (0.02λ) to reduce the radiation loss. The solid ground plane separates the antenna and the

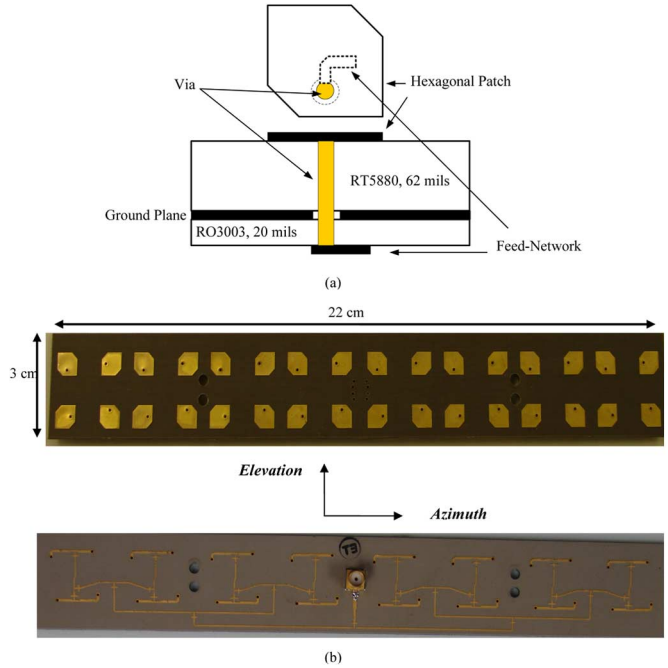

Fig. 2. (a) Top-view and side-view of an array element, showing its two-layer substrate. (b) 2 × 16 fabricated sub- array antennas and its feed-network.

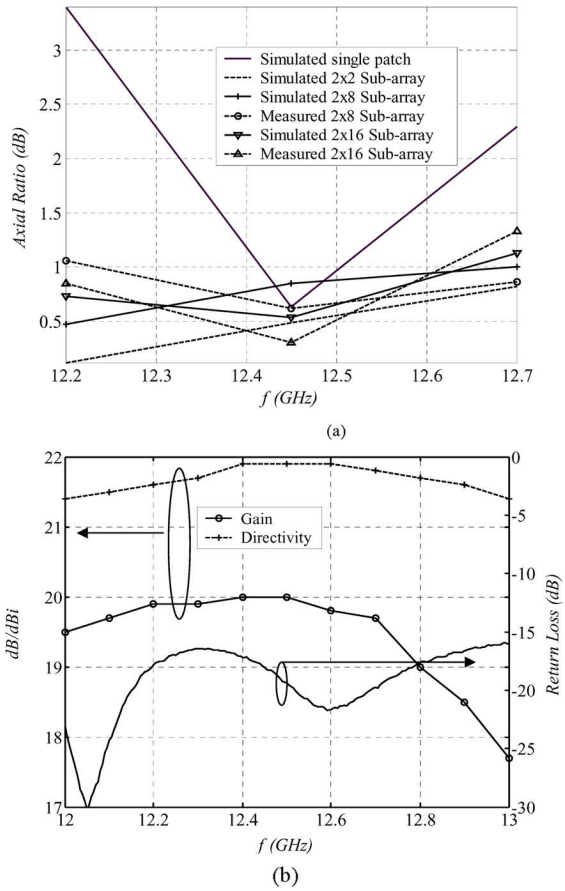

Fig. 3. (a) Simulated axial ratio of a single element, 2 × 2, 2 × 8, and 2 × 16 sub-array antenna and measured axial ratio for 2 × 8,and 2 × 16 sub-array antennas. (b) Measured input matching for 2 × 16 sub-array antenna and the measured radiation gain and directivity of 2 × 16 sub-array antenna versus frequency.

feed-network, reducing the adverse effect that the antenna and the feed-network may have on each other. The feed-network is connected to the patch by a via-pin that passes through a hole in the ground plane. The via-pin allows access to the point inside the patch which has a lower input impedance compared to the points at the edge of the patch. This leads to a better impedance matching and a lower insertion loss within the feed-network.

To design the element, we have taken advantage of Agilent Momentum which applies the method of moments to the mixed-potential integral equation (MPIE) of multilayer media. To guarantee the desired performance over the bandwidth of interest, gain, axial ratio, and VSWR are calculated over the entire bandwidth. According to these results, the optimum element has a radiation gain of 6.7 dBi and an axial ratio of less than 3.5 dB [Fig. 3(a)] over the relative bandwidth of 4%. The patch has VSWR of 1.4:1 on the 50 Ω line over the operating frequency.

Although the achieved element gain is satisfactory, the axial ratio of 3.5 dB is not acceptable for this application. To improve the axial ratio further, we have used four elements with sequential rotation of 0°, 90°, 180°, and 270° in space. This spatial rotation must be compensated for by a corresponding electrical phase shift to retain circular polarization and to achieve an axial ratio better than that of a single element. This technique of improving axial ratio has been previously described in [13] and recently has been used for similar array applications in [14], [15]. The axial ratio for sequentially-rotated four elements (2 × 2) is given in Fig. 3(a) (it includes the feed network effect). It has been observed that the designed four-element array has an axial ratio of less than 1 dB over a relative bandwidth of 4%. This four-element array has then been used as a building block for formation of 2 × 8 and 2 × 16 sub-arrays.

Fig. 2(b) shows the fabricated 2 × 16 sub-array and its feed-network (2 × 8 sub-array has similar configuration with half number of elements). The 2 × 16 sub-array size is 22 cm × 3 cm. The input scattering parameters of the 2 × 16 sub-arrays are measured and demonstrated in Fig. 3(b). It is apparent that a good matching is achieved over a wide range of frequencies. The present results are obtained by using surface mount SMA connector.

The radiation characteristics of these sub-arrays are measured using near-fields techniques. Fig. 4(a) and (b) illustrate the results of these measurements in the principal azimuth and elevation planes of the sub-array at 12.7 GHz. These planes are defined in Fig. 2. The measured circular polarization gain of the 2 × 16 sub-array is about 19.7 dBi and that of 2 × 8 is 17.4 dBi. The loss added by the surface mount connector is estimated to be 0.5 dB at this frequency range. Therefore, the actual gains are 20.2 dBi and 17.9 dBi for the 2 × 16 and 2 × 8 sub-arrays, respectively at 12.7 GHz. The gain and the directivity of the 2 × 16 array are measured from 12 to 13 GHz and are shown in Fig. 3(b). The difference between them is 1.8 dB which is the loss of feed-network and the SMA connector. Subtracting the SMA connector loss, the feed-network loss is 1.3 dB. Therefore, the gain of 2 × 16 sub-array is varying between 20.5 dBi and 20.2 dBi when the effect of SMA connector is excluded. The half power beam width (HPBW) in elevation according to Fig. 4(a) and (b) is approximately ±20 degrees for both 2 × 8

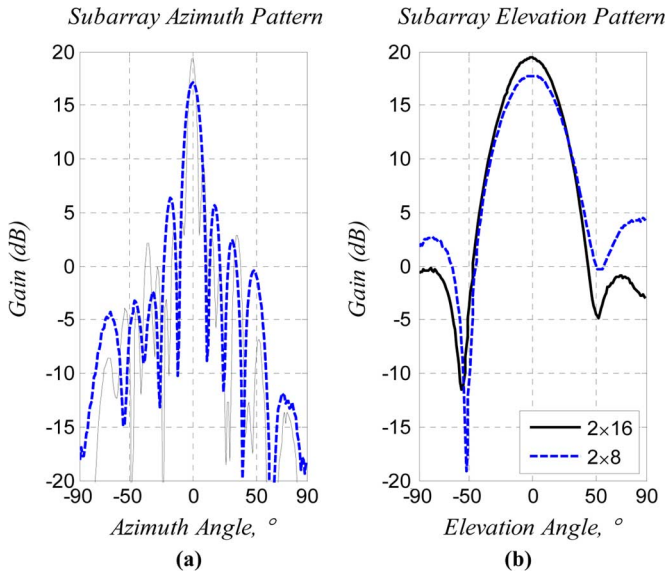

Fig. 4. Measured radiation patterns of 2×8 and 2×16 sub-arrays f = 12.7 GHz. (a) Azimuth plane. (b) Elevation plane.

and 2×16 sub-arrays. The azimuth HPBWs are ± 4.6 degrees and ± 2.8 degrees for 2×8 and 2×16 sub-arrays, respectively.

The sub-arrays axial ratios are also measured from the spinning linear pattern and are compared with the simulation [Fig. 3(a)]. For both 2×8 and 2×16 sub-arrays the axial ratios are less than 1.4 dB and for most of the operating band is less than 1 dB.

B. Low Noise Amplifier Transition to Sub-Array

Due to the loss associated with the cable and phase shifter/power combiner, it is necessary to add a low noise amplifier (LNA) to each sub-array. This requires assembly of a large number of LNAs and sub-arrays which renders the use of vast number of connectors and significant amount of labor to connect them. Also each LNA should be located very close to the corresponding sub-array in order to reduce the loss and fix the noise figure of that channel through the rest of the path down to the mixer. Therefore, developing a method to connect the LNA and sub-arrays is an important step to reduce the assembly cost, increase the reliability and improve the overall G/T of the phased array antenna.

In this paper, we don't intend to go through the details of the LNA design as it is a rather standard design. However, a transition between sub-array antenna and LNA will be explained. Here a new transition structure in the form of two stage coaxial lines is designed in the housing of the LNA. This method is based on the direct connection of the LNA to the corresponding antenna sub-array which allows the vertical transmission of signal energy to the input of the LNA.

The output of the sub-array feed-network needs to be transferred to the co-planar waveguide (CPW) transmission line which is more appropriate for vertical transition to the two stage coaxial line. To do this the microstrip line width would change and through a matching stub it converts to the CPW transmission line as shown in Fig. 5(a). The ground planes of CPW are connected to the ground plane of the microstrip feed-network

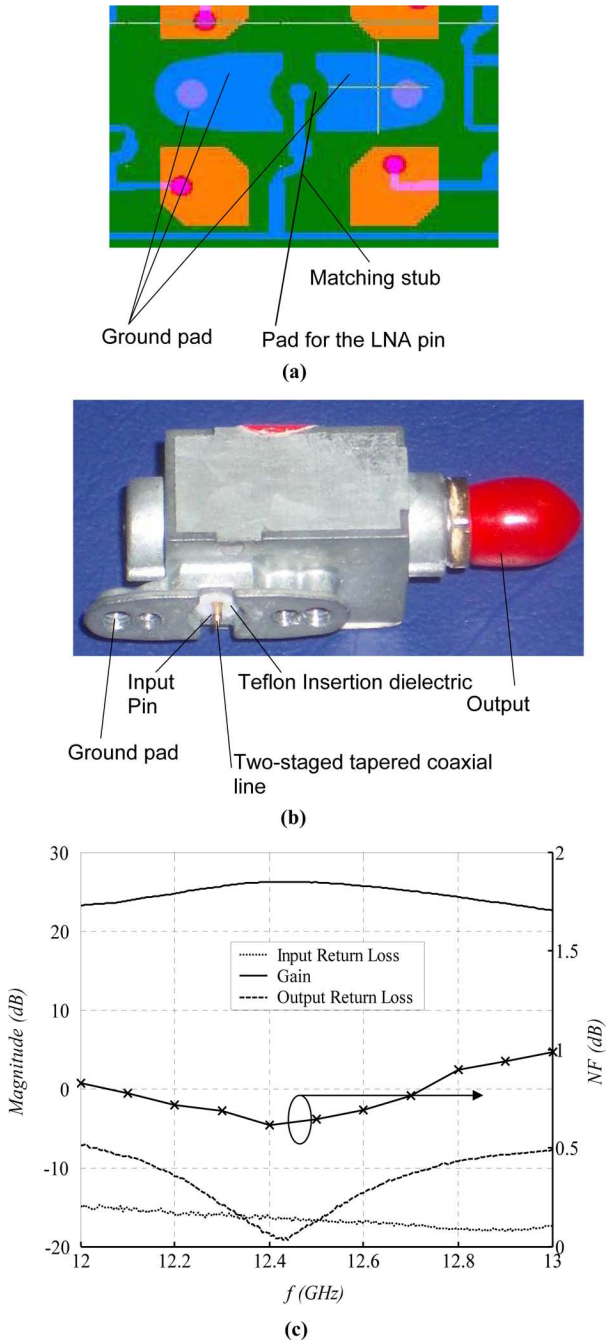

Fig. 5. Low noise amplifier transition to sub-array: (a) Large view of the sub-array port with matching circuit, (b) fabricated model, (c) measured parameters for the fabricated LNA.

and the antenna patches (Fig. 2) through via-pins. The middle ground pad is perforated (circular shape) to accommodate for coaxial line medium in the LNA housing [Fig. 5(a)]. The amount of perforation is optimized to provide the minimum VSWR. The signal line terminated to the circular pad which is large enough to allow installation of the central (signal) pin of the input of the LNA in Fig. 5(b).

The LNA has two compartments: one for allocating the DC bias circuitry, and the other one for microwave circuits shown in Fig. 5(b). The two stage coaxial line embedded in the housing of the LNA is terminated to a microstrip line in the microwave

compartment which immediately is connected to the gate of the first stage transistor. The other side of the pin is connected to the circular pad of CPW on the feed-network substrate. The first stage of the coaxial line is filled with low loss dielectric. The dielectric is also used to maintain the signal pin. On the second stage the diameter of the outer conductor of the coaxial line increased and the dielectric is removed. This allows smooth transition to the CPW line on the feed-network side. The length of the second stage coaxial is selected in the way that metallic ceiling on the step which is parallel to the feed-network ground plane to be significantly taller compared to the feed-network substrate thickness. This would result in reducing capacitive parasitic effect which changes the feed-line characteristic. The housing pad of the LNA would be soldered or attached by conductive glue to the CPW ground plane. The second stage is also designed and optimized to allow the insertion of standard female type SMA connector for the test and qualification purposes.

The fabricated LNA was tested using network analyzer (Agilent 8722ES) and noise figure analyzer (Agilent N8975A). The measured parameters are shown in Fig. 5(c). The gain of the LNA is about 25 dB with input and output return loss of better than -10 dB over the band of operation. The noise figure is less than 0.8 dB over the band.

C. Analog Phase Shifter

The challenges in the phase shifter design for low cost mobile satellite phased array antennas are as follows [16].

1) Achieving phase linearity: This is a complicated task for MIC implementation at Ku-band as the required minimum varactor capacitance becomes comparable to the parasitic capacitance;
2) The circuit layout should avoid infinitesimal critical dimension to achieve high yield and reduce the manufacturing cost;
3) Low complex phase control: minimum control complexity with very few number of control voltages is required to reduce the number of digital/analog converters (DAC).

Fig. 6(a) shows the circuit topology of the reflective-type phase shifter (RTPS) consisting of a 3-dB 90-degree hybrid coupler and a low loss reflective load connected to its through and coupled ports while the other ports are symmetrically matched to the 50 Ω input and output. The phase of RTPS can be controlled by changing the impedance of the reflecting load. This can be done by varying the capacitance $\mathrm{C_v}$ between $\mathrm{C_{min}}$ and $\mathrm{C_{max}}$. The absolute value of this phase variation is given by

$$\Delta\varphi = 2|\arctan(Z_{\max}/Z_o) - \arctan(Z_{\min}/Z_o)| \qquad (4)$$

where $Z_{\min}$ and $Z_{\max}$, show the maximum and the minimum of input impedances of the reflective load and Z_o is the characteristic impedance of the line.

The phase shift introduced by a varactor alone is limited [17]. The phase control range can be increased by resonating the varactor with a series inductor at their resonance frequency. However, at Ku-band the required minimum amount of varactor capacitance to produce the phase shift in excess of 180° is less than 50 fF, which is of the same order as the package and connection parasitic capacitances for MIC implementation [Fig. 6(b)]. These parasitic capacitances have dramatic effects on the phase shift linearity and may result in flattening of the C-V and consequently on the termination reactance characteristics, respectively.

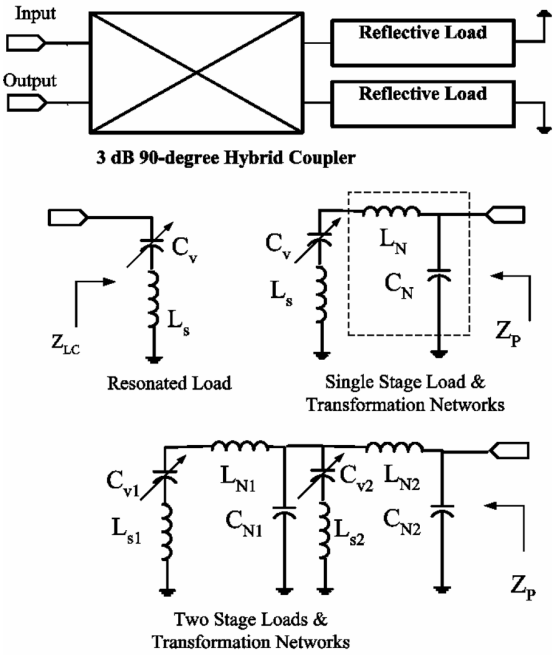

Fig. 6. (a) Phase shifter topology of RTPS with different reflective loads and (b) phase shift for reflective LC load and LC with impedance transformer.

To solve this problem, an impedance transformer network is added to L-C series resonance networks as shown in Fig. 6(a). This network transforms the load impedance (Z_{LC}) to a larger value $(\mathrm{Z_p})$ according to

$$Z_p = Q^2 Z_{\mathrm{LC}} \qquad (5)$$

where Q is the quality factor of the network. This network increases the minimum required varactor capacitance to 135 fF, well above those aforementioned parasitic capacitances. Also, as shown in Fig. 6(b), it reduces the required varactor tuning

range. Another effect of this network is to decrease the variation of the magnitude and as a result reduce the loss variation of the phase shifter.

A single stage phase shifter was designed at the center frequency of 12.5 GHz. In this design we used commercially available GaAs hyper-abrupt junction varactor diodes with constant Gamma of 1.25 and series resistance of $R_{\rm S} = 3.5\ \Omega$. The capacitance varies from 1.0 pF to 0.10 pF by varying the DC bias voltage from 0 to 12 volts, respectively. The operating temperature range is from -50°C to 150° C which is ideal for land mobile satellite links.

Two stage reflective loads shown in Fig. 6(a), are used to maximize the insertion phase and minimize the insertion loss variation. The load inductors, $L_{\rm S}$, are fabricated using vias to ground with diameter of 0.8 mm. The values of the inductors are 0.24 nH. The impedance transformer networks (reflective loads) are designed using stepped microstrip line. The phase shifter simulation was performed using ADS software.

Fig. 7(a) shows a fabricated single stage phase shifter. It was tested using network analyzer (HP 8722ES). Fig. 7(b) shows the measured phase shift for this device. The phase shift of 376 degree was obtained over 12.0 to 13.0 GHz by changing the control voltage from 2 to 10 volts which corresponds to the capacitance variation between 0.47 to 0.13 pF, respectively. The phase shift variation over the operating frequency is only 10 degrees. Compared to the measurement results of [18] it has four times larger bandwidth and less phase shift variation over the band of operation with the voltage variation of only 8 volt. The latter is important for the operation on a vehicle with 12 volts battery.

Fig. 7(c) illustrates the measured insertion loss. In the measurement the effect of SMA connectors and DC block capacitors are also included. By subtracting these losses ($\sim$1 dB) the total insertion loss of the circuits becomes -3.2 ± 0.8 dB (for 12.2 to 12.7 GHz). Fig. 7(c) also demonstrates the measured return loss, which is better than -10 dB in the whole range of frequency (12.2 to 12.7 GHz). In this configuration, the bandwidth of the phase shifter in terms of return loss and insertion loss, are mostly dominated by the 3-dB hybrid coupler. The bandwidth can be improved by using Lange coupler.

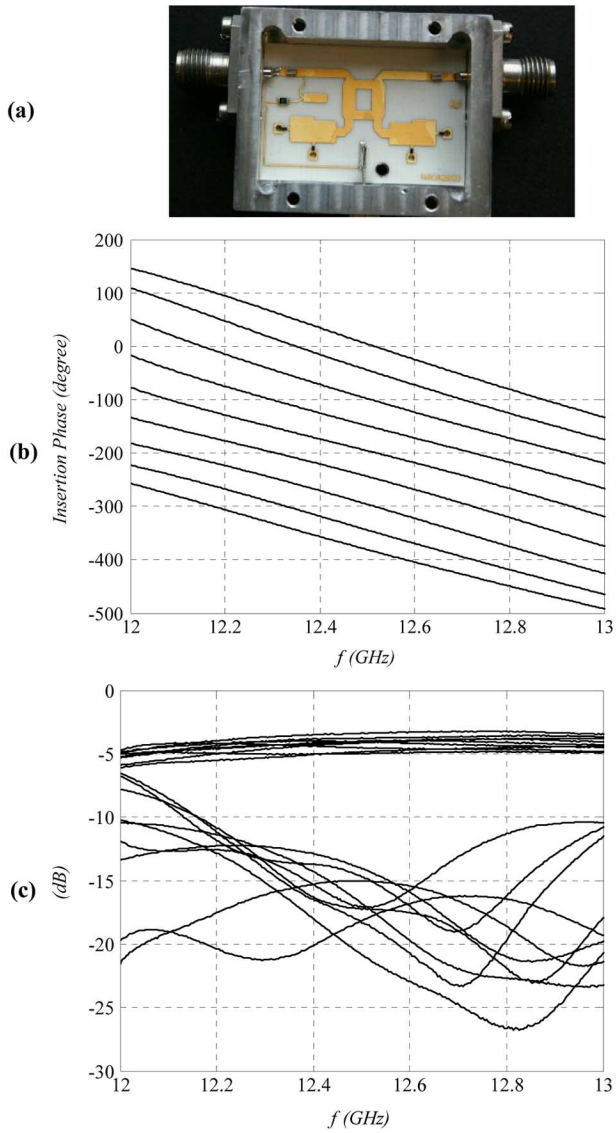

Fig. 7. (a) Fabricated phase shifter, (b) measured insertion phase, and (c) measured return and insertion loss.

IV. Hybrid Tracking

Conventionally, the satellite tracking can be divided into two modes, i.e., *initial satellite search mode* and *tracking mode*. A *re-initialization mode* can also be foreseen for the cases when the satellite signal is lost for a period of time due to blockage or signal shadowing, and an initial search is required to retain the lock. In the initial satellite search mode, which is hereinafter called "*Homing*", the antenna beam is pointed towards the desired satellite by means of rotating the antenna or its beam. In the tracking mode the antenna tracks the satellite by compensating for the vehicle movement. In this mode, it is likely that the satellite tracking system loses track of the satellite direction during signal outage, e.g., when the satellite view is temporarily blocked by a large object or when the vehicle passes through tunnels. To alleviate this problem and retain the satellite lock, the homing mode should be reperformed. To differentiate this mode from initial homing it is called *Re-Homing*.

In the tracking mode of the phased array antenna system, two complementary mechanisms operate simultaneously: the stabilization loop and an electronic beamforming. The stabilization loop is mostly responsible for keeping the antenna toward a pre-determined attitude during sharp maneuvers of the vehicle. A low-cost MEMS rate gyro, mounted on the antenna platform, provides most of the information required by the loop. However, the low-cost MEMS sensor suffers from high rate drift and strong noise. Role of the electronic beamforming is to compensate for the sensor irregularities. It plays as an external aid for the stabilization loop and eliminates the residual azimuth angle error. Moreover, integrating the two mechanisms enables the tracking system to nullify slow angular disturbances even those hidden within the noise of the gyro. In the following after a brief description regarding the antenna initial homing, structure of the stabilization loop is given. The electronic beamforming procedure is consecutively presented in Section IV.C.

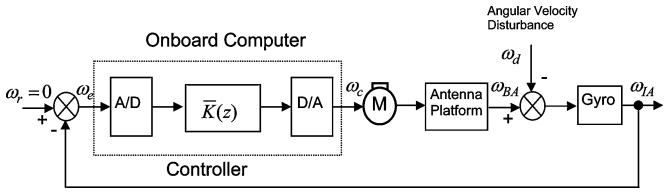

Fig. 8. Block diagram of the stabilizing loop.

A. Homing Mode

In the homing mode the search starts with a preset phase shifters setting, obtained from the history of the system from last operation. This setting includes the initial values for the control voltages of the phase shifters. Using two step motors, the mechanical search is performed in both azimuth and elevation. Upon exceeding an RF power threshold, the control system extracts the satellite ID and compares it with the desired satellite ID. As the power of the received signal depends on the environmental conditions and the vehicle position, the mentioned RF power threshold should be set adaptively. The adaptive threshold setting and checking of the good RF power level are done by performing moving averaging for the signal power with two different averaging window sizes. The corresponding moving averages are named *short term averaging* and *long term averaging* based on the window size. The long term averaging is used for setting the adaptive RF power threshold level. The short term averaging value, on the other hand, is compared with the long term one to check for the good signal level. After locking to the desired satellite, the homing control system performs a fine tuning to maximize the received RF power as much as possible.

In order to compensate for the vehicle movement in homing mode, the azimuth gyro control loop is activated during this mode. This helps the system find the desired satellite as fast as possible at all times during which the vehicle is moving.

B. Stabilization Loop

Structure of the stabilization loop is given by Fig. 8. It is a custom-designed real time embedded micro-processor control system. As illustrated by the diagram, the digital controller $\bar{K}(z)$ is driven by the stabilizing loop error ω_e; that is the perturbed angular velocity of the antenna platform from the desired angular velocity of $\omega_r = 0$ which is measured by the gyro. Manipulating the stabilizing loop error, it produces suitable commands to the motor driver circuit to nullify the angular velocity disturbance ω_d. The controller $\bar{K}(z)$ is designed to provide a slightly under-damped controlled response with a Maximum Percent Over-Shoot (MPOS) not more than 15%. It is also required to offer a closed-loop bandwidth of about 30–35 rad/sec.

C. Electronic Beamforming

After the Homing mode was performed successfully, the system continuously tracks the satellite by monitoring the yaw rate sensor readings. However, the gyro's high rate drift gradually deflects the antenna platform from the desired attitude. On the other hand, some slow-rate disturbances can not even be felt by the low-cost gyro. The electronic beamforming is aimed to maximize the array output power, and compensate for the angular rate sensor inaccuracies by tracking the relative satellite displacements caused by small vehicle movements within a predefined window. For large vehicle movements, however, a mechanical control loop is needed to point the antenna towards the desired satellite and keep the antenna position inside the window for which the electronic beamforming is effective.

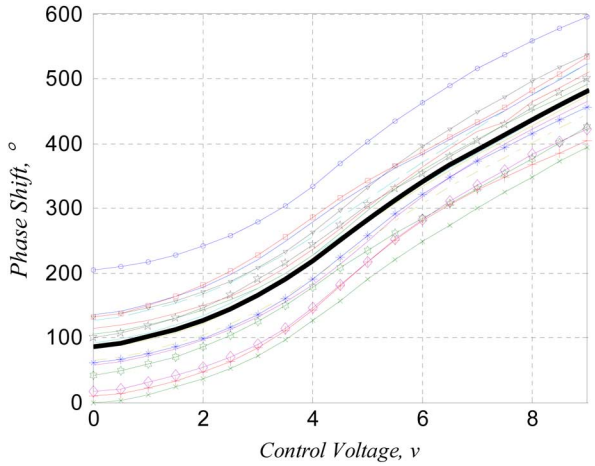

Fig. 9. Phase-Voltage characteristics of 17 channels of the phased array antenna. Each channel includes an analog phase shifters, a cable and a LNA. The dark solid line shows the average of all curves.

Electronic beamforming is the essential part of both homing and tracking modes. To implement this technique prior knowledge of the phase-voltage characteristics of each channel (LNA + cable + phase shifter) is required. As these characteristics are device dependent (see Fig. 9), and may change with the environmental conditions, such as temperature and humidity, as well as aging, a non-model based algorithm for the beamforming is required. To this end, an innovative beamforming technique is devised which does not require the system model parameters in general. This technique is referred to as the *zero-knowledge beamforming* [8].

The goal of beamforming is to set the control voltages of the phase shifters in such a way that the received signal from the satellite is maximized. This problem can be solved using gradient based optimization techniques which require an estimation of the array correlation matrix. To estimate the correlation matrix the signals from all antenna arrays may be required, which are accessible only when the base-band processing is employed. However, in the case when a combined signal from all antenna arrays is the only source, the problem becomes more complicated. To solve this problem we resort to the *perturbation methods* in order to estimate the gradient from the combined RF received signal. In the following the zero-knowledge beamforming algorithm is described.

Fig. 10(a) shows the simplified block diagram of the beamforming network. Let $\mathbf{s}(n) = [s_1(n), s_2(n), \ldots, s_N(n)]$ and $\mathbf{w}(n) = [w_1(n), w_2(n), \ldots, w_N(n)]$ denote the impinged signal from the target to the array elements and the phase shifts applied to each antenna element at time instant n, then the total signal after the power combiner is given by

$$f(n) = \mathbf{w}^*(n)\mathbf{s}^T(n) \tag{6}$$

where $*$ and $^{\mathrm{T}}$ denote the complex conjugate and transpose operations, respectively. The measured RF power at the output of the RF detector, which is a logarithmic amplifier measuring the received power over the whole IF spectrum, is

$$P(n) = K_0 \log\{E[f(n) \cdot f^*(n)]\} \tag{7}$$

where $\mathrm{E}[\cdot]$ denotes the expectation operation, and K_0 is the amplification gain. Note that $P(n)$ is a function of the phase shifts applied to each antenna element, i.e., $\mathbf{w}(n) = [w_1, w_2, \ldots, w_N]$. In general, these phase shifts are controlled by a set of control voltages which can be shown by a $1 \times N$ vector as $\mathbf{v}(n) = [v_1, v_2, \ldots, v_N]$, and

$$w_i(n) = f[v_i(n)] \cdot \exp[j\psi(v_i(n))] \tag{8}$$

where f and ψ are two functions of the control voltage. To maximize the array output power a Least Mean Square (LMS) technique can be employed. In such methods, however, a direct unbiased measurement of the gradient,$\mathbf{g}(\mathbf{v}) = \nabla P$, is required. In single receiver phased arrays the only source of the received information is the RF signal power, from which the gradient cannot be measured directly. Hence, we explore the stochastic approximation and the finite-difference (FD) method in order to estimate the gradient vector,$\mathbf{g}$, using noisy measurements of the array output power. Based on this method the recursive zero-knowledge beamforming algorithm can be formulated as

$$\mathbf{v}(n+1) = \mathbf{v}(n) + 2\mu\hat{\mathbf{g}}(n) \tag{9}$$

where μ is a positive scalar indicating the *step-size* which controls the convergence rate, $\hat{\mathbf{g}}(n) = [\hat{g}_1(n), \hat{g}_2(n), \ldots, \hat{g}_N(n)]$ is the estimated gradient vector, and n shows the discrete time index. Using a two-sided finite difference technique, the ith element of the estimated gradient vector is calculated as

$$\hat{g}_i(n) \approx \frac{P(v_i(n)+\delta) - P(v_i(n)-\delta)}{2\delta}. \tag{10}$$

In (10), δ denotes the perturbation added/subtracted to the control voltages to find the finite difference approximation of the partial derivatives. As it is seen from (9) and (10) the performance of the beamforming algorithm is determined by the step size and perturbation parameters, μ and δ. Considering the convergence rate and the steady state error as performance measures, the proper values of step size and perturbation are obtained through an extensive simulation study.

Fig. 10(b) demonstrates the functional block-diagram of the beamforming process. The first step is to perturb the control voltage v_i, and update all phase shifters. Next the RF detector output is filtered using digital and analog low pass filters to reduce the effect of noise, and next, the received power is measured. This process is repeated for each element if a sequential perturbation is used to estimate the gradient vector $\hat{\mathbf{g}}(n)$, there are other perturbation methods with a lower number of perturbations [20]. The beamforming process needs to be run for a few iterations to guarantee the convergence of the received power.

During the fine tuning the electronic beamforming directs the phased array antenna beam towards the satellite. Based on the vehicle movement, the direction of the beam may not coincide

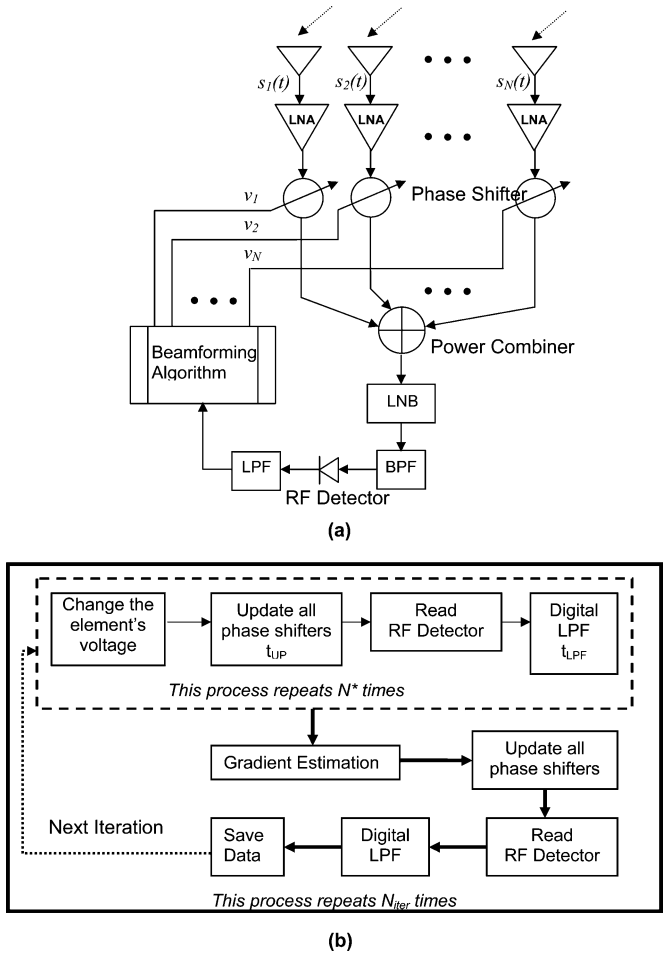

Fig. 10. The phased array antenna beamforming network: (a) block diagram, (b) flow chart of the beamforming algorithm.

with the antenna broadside pointing direction. Monitoring the values of the phase shifters control voltages is a way to estimate the direction which antenna should rotate in order to get the maximum RF power in the broadside. Based on these voltages the direction is estimated employing some pre-set rules [19]. These rules specify which direction the antenna system should rotate in order to make the main lobe of the antenna perpendicular to antenna elements surface.

V. Experimental Results

Different measurements were made to test the phased array antenna performance. The phased array antenna system was mounted on a test vehicle (Fig. 11). The system parameters were monitored and registered in a laptop. The output of the antenna system was connected to a satellite receiver and TV and the satellite signal strength was monitored by the receiver signal quality indicator (*bar*). The tests were conducted in Waterloo, Ontario Canada with the elevation angle of around 35° for the Bell Expressvu 91 satellite.

First the homing mode was tested when the vehicle was at rest. In this static homing mode, the motor rotates the antenna with an angular speed of 45 deg/s. Neglecting the time required to extract the undesired satellites ID's, the homing process takes at most 14 seconds, which includes the times required to scan

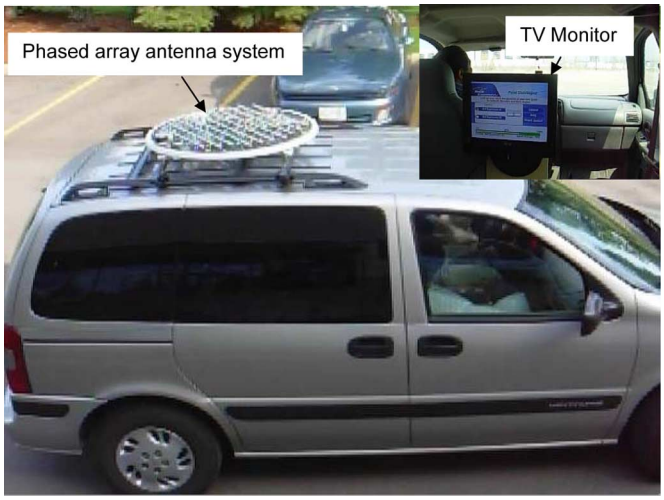

Fig. 11. The phased array antenna system mounted on a test vehicle.

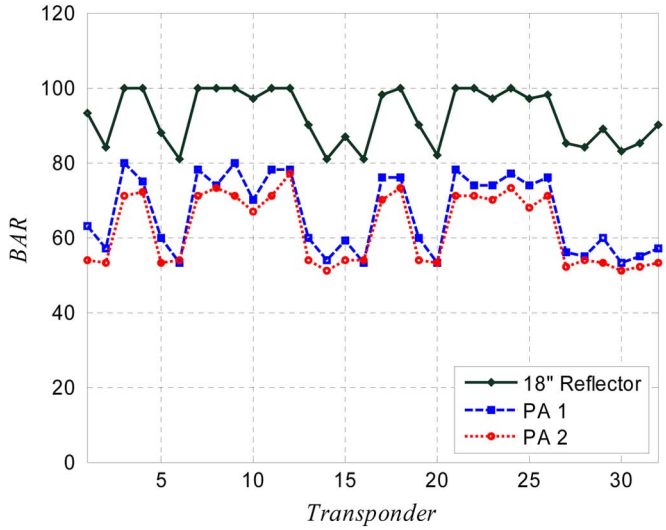

Fig. 12. The comparison of measured signal strength from Bell ExpressVu91 receiver for two phased array antenna (PA) and a standard 18 inch reflector antenna.

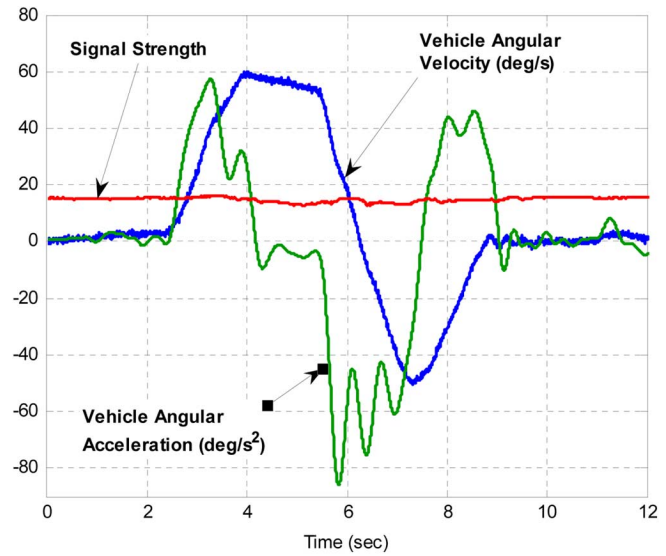

Fig. 13. The performance of the phased array antenna in a road test.

360 degrees in azimuth and extract the desired satellite ID from the received signal. The real homing time depends on the initial position of the antenna and the number of undesired satellites between the initial position and the desired one. As extracting each satellite ID takes around 6 seconds, the number of the undesired satellites affects the homing process duration. The test results show that on average the homing can be completed in 35 seconds.

Upon being locked on the desired satellite (Bell Expressvu 91), the signal quality for different transponder was measured and compared with that of an $18''$ commercial off-set reflector antenna. Fig. 12 compares the signal qualities of the phased array antennas and a reflector antenna. The figure shows the signal quality[1] of the phased array antennas for different transponders follow the same trend as the reflector one. As the reflector is a wide band antenna, an immediate conclusion is that the performance of the phased array antenna does not vary with frequency as well.

The tracking system agility was measured by a road test. In order to monitor the test vehicle maneuver an auxiliary gyro was installed in the fixed part of the antenna platform. Manipulating the auxiliary gyro's signal the velocity and the acceleration of the vehicle during the road test were calculated. Along with these parameters the scaled output of the RF detector was registered. Fig. 13 shows a typical result when the vehicle veered away to the left and right. As the results show the RF signal level stays almost fixed even if the vehicle makes sharp turns with high angular velocities around 60 deg/s.

During the road tests we observed that the antenna system tracks the satellite even in the uphill/downhill roads and flat roads with abrupt bumps without using mechanical tracking in elevation. This is mainly due to the broader antenna beam-width in the elevation plane and the strength of the beamforming. To elaborate more, we can argue as follows. If the target moves relative to the phased array axes, the beamforming algorithm is capable of steering the beam toward the target such that the array factor remains at its maximum value. Therefore any drop in the total received power or radiation gain is due to the radiation pattern of the elements. Fig. 14(a) shows the radiation pattern of the whole array when the target moves $\pm 10^\circ$ in elevation relative to the array normal axis. Since the radiation pattern of the elements is fairly wide in elevation, the maximum gain drop is less than 1 dB. However since the radiation pattern in azimuth is narrow, as Fig. 14(b) illustrates, the maximum angular shift of the target in azimuth without a significant drop in gain is much smaller, around $\pm 2^\circ$.

[1]The signal quality is measured based on the bar indicator of the satellite receiver which indicates the received signal-to-noise level at the base-band.

VI. Conclusion

An ultra low-profile and low cost phased-array antenna structure with two dimensional electronically scanning capability was introduced and the design procedures of its components

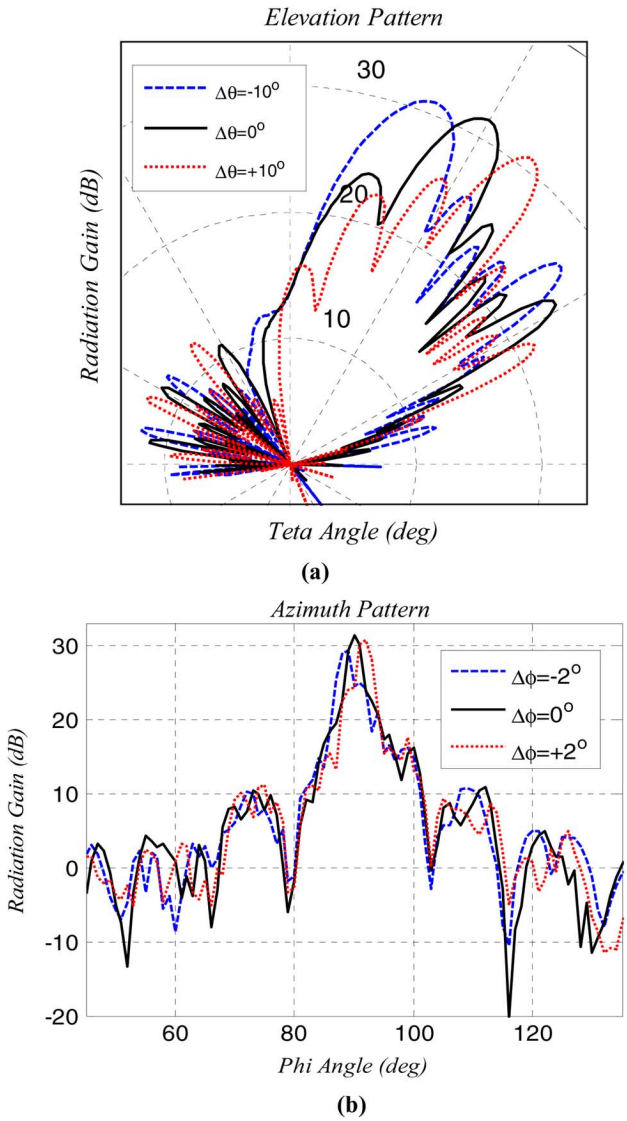

Fig. 14. The radiation pattern of the phased array antenna: (a) in the elevation plane for three different target locations (the mechanical angle of the antenna is fixed at 30°) and (b) in the azimuth plane for three different target locations (the mechanical angle of the antenna is fixed at 90°).

were discussed in detail. The total system weight and physical dimensions make the installation of this system on any regular vehicle possible. The mobile phased-array antenna receives LHCP and RHCP signals simultaneously with a total radiation gain of 31.5 dB. In order to compensate for the inaccurate and low cost system components, such as the analog phase shifters and rate gyro, a novel hybrid tracking algorithm was introduced based on zero-knowledge beamforming. Thanks to this beamforming algorithm the main-beam can be steered to $\pm 2.8^\circ$ in azimuth and $\pm 20^\circ$ in elevation during a few milliseconds. The azimuth gyro compensated the coarse movement of the antenna platform, while the fast electronic beamforming algorithm enabled the antenna to respond much faster and prevented the mechanical system to be engaged all the time. The real time road tests were performed in order to verify the agility of the phased-array system. The tracking system was able to track the satellite even when the vehicle made fast turns and can nullify the base vehicle yaw disturbances up to 60 deg/s and 85 deg/s^2. The quality of the received signal in different weather condition was proven to be satisfactory and comparable with 18-inch dish antenna through hundreds of off-board and on-board tests.

REFERENCES

[1] Y. Ito and S. Yamazaki, "A mobile 12 GHz DBS television receiving system," *IEEE Trans. Broadcasting*, vol. 35, no. 1, pp. 56–62, Mar. 1989.

[2] A. C. Densmore and V. Jamnejad, "A satellite-tracking K- and Ka-band mobile vehicle antenna system," *IEEE Trans. Veh. Technol.*, vol. 42, no. 4, pp. 502–513, Nov. 1993.

[3] Mccarrick and C. Charles, "Offset stacked patch antenna and method," U.S. Patent 7102571, Sep. 3, 2006.

[4] I. Stoyanov, V. Boyanov, B. Marinov, Z. Dergachev, and A. Toshev, "Mobile Antenna system for satellite communications," U.S. Patent 6999036, Jul. 12, 2005.

[5] J. Hirokawa, M. Ando, and N. Goto, "A single layer slotted leaky waveguide array antenna for mobile reception of direct broadcast from satellite," *IEEE Trans. Veh. Technol.*, vol. 44, no. 4, pp. 749–755, Nov. 1995.

[6] S. Jeon, Y. Kim, and D. Oh, "A new active phased array antenna for mobile direct broadcasting satellite reception," *IEEE Trans. Broadcasting*, vol. 46, no. 1, pp. 34–40, Mar. 2000.

[7] S. Y. Eom, S. H. Son, Y. B. Jung, S. I. Jeon, S. A. Ganin, A. G. Shubov, A. K. Tobolev, and A. V. Shishlov, "Design and test of a mobile antenna system with tri-band operation for broadband satellite communications and DBS reception," *IEEE Trans. Antennas Propag.*, vol. 55, no. 11, pp. 3123–3133, Nov. 2007.

[8] M. Fakharzadeh, S. Safavi-Naeini, S. H. Jamali, and P. Mousavi, "Zero-knowledge beamforming of phased array antennas based on simultaneous perturbation gradient approximation," in *Proc. IEEE Int. Symp. Antennas Propag.*, Albuquerque, NM, Jul. 2006, pp. 537–540.

[9] M. Fakharzadeh, P. Mousavi, S. Safavi-Naeini, and S. H. Jamali, "The effects of imbalanced phase shifters loss on phased array gain," *IEEE Antennas Wireless Propag. Lett.*, to be published.

[10] J. J. Lee, "G/T and noise figure of active phased array antenna," *IEEE Trans. Antennas Propag.*, vol. 41, no. 2, pp. 241–244, Feb. 1993.

[11] P. S. Hall, J. Huang, E. Rammos, and A. Roederer, "Gain of circular polarized array composed of linearly polarized elements," *Electron. Lett.*, vol. 25, pp. 124–125, Jan. 1989.

[12] J. Huang, "A Ka-band circularly polarized high-gain microstrip array antenna," *IEEE Trans. Antennas Propag.*, vol. 43, no. 1, pp. 113–116, Jan. 1995.

[13] P. S. Hall, "Review of techniques for dual and circularly polarized microstrip antenna," in *Microstrip Antennas: The Analysis and Design of Microstrip Antennas and Arrays*, D. M. Pozar and D. H. Schaubert, Eds. New York: IEEE Press, 1995.

[14] C. Wnng and K. Chang, "A novel CP patch antenna with simple feed structure," in *Proc. IEEE Antennas Propag. Soc. Int. Symp. Dig.*, Jul. 2000, vol. 2, pp. 1000–1003.

[15] N. C. Karmakar and M. E. Bialkowski, "Circularly polarized aperture-coupled circular microstrip patch antennas for L-band applications," *IEEE Trans. Antennas Propag.*, vol. 47, no. 5, pp. 933–940, May 1999.

[16] P. Mousavi, I. Ehtezazi, S. Safavi-Naeini, and M. Kahrizi, "A new low cost phase shifter for land mobile satellite transceiver," in *Proc. IEEE Int. Symp. Antennas Propag.*, Jul. 2005, pp. 229–232.

[17] S. Hopfer, "Analog phase shifter for 8–18 GHz," *Microw. J.*, no. 3, pp. 48–50, Mar. 1979.

[18] S. Shin, R. V. Snyder, and E. Niver, "360-degree linear analog phase shifter design using short-circuit terminated combline filters," in *IEEE MTT-S Int. Microw. Symp. Dig.*, May 2001, vol. 1, pp. 303–306.

[19] M. Fakharzadeh, S. Safavi-Naeini, S. H. Jamali, P. Mousavi, and K. Narimani, "Accurate limited angle tracking with a phase array antenna using zero-knowledge beamforming," in *Proc. IEEE Int. Symp. Antennas Propag.*, June 2007, pp. 1104–1107.

[20] M. Fakharzadeh, H. Jamali, S. Safavi-Naeini, P. Mousavi, and K. Narimani, "Fast stochastic beamforming for mobile phased array antennas," in *Proc. IEEE AP-S Int. Symp. Antennas Propag.*, Honolulu, HI, pp. 1945–1948.

Pedram Mousavi (S'96–M'01) received the B.Sc. (Hons.) degree in telecommunication engineering from Iran University of Science and Technology, Tehran, in 1995 and the M.Sc. and Ph.D. degrees from the University of Manitoba, Winnipeg, Canada, in 1997 and 2001 respectively, all in electrical engineering.

From 2001 to 2003, he was a Senior Microwave Engineer with Sirific Wireless Corp. where he worked on the development of multiband VCO for various wireless standards. From 2003 to 2004, he was a Postdoctoral Fellow with the Department of ECE and the Centre for Integrated RF Engineering at the University of Waterloo, Waterloo, ON, Canada, conducting research on low cost low profile phased array antenna system for mobile satellite communication. Based on his research at the University of Waterloo he founded Intelwaves Technologies of which he is currently the CEO. Intelwaves Technologies Ltd. is developing a comprehensive suite of smart antenna technologies that can be used to provide satellite TV programming and satellite broadband Internet access within moving vehicles, from passenger cars to commercial aircrafts. Their vision is to make cars a communication center. His research interest includes miniaturized intelligent antennas and radios, microwave and millimeter wave low profile/integrated adaptive antenna structures, and emerging technologies for microwave and millimeter wave in smart antennas.

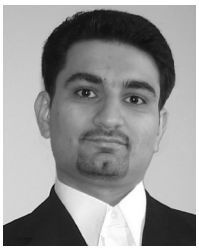

Mohammad Fakharzadeh received the B.Sc. degree in electrical engineering (honors) from Shiraz University, Shiraz, Iran and the M.Sc. degree from Sharif University of Technology, Tehran, Iran, in 2000 and 2002, respectively.

From January 3 to September 4, 2003, he was a faculty member in the Electrical Engineering Department, Chamran University of Ahvaz, where he was evaluated as the Best Instructor by the undergraduate students of the department. Currently he is a member of the Intelligent Integrated Radio and Photonics Group, University of Waterloo, Waterloo, ON, Canada, working toward the Ph.D. degree. His areas of interest include phased array design and beamforming, optical delay lines, signal processing and adaptive filters.

S. Hamidreza Jamali was born in Zanjan, Iran. He received the B.Sc. and M.Sc. degrees from the University of Tehran, Tehran, Iran, in 1978 and 1980, respectively, and the Ph.D. degree from Concordia University, Montreal, QC, Canada, in 1991.

From 1982 to 1983, he was with the Electronics Research and Production Center, a subsidiary of the Iran Broadcast Organization. In 1983, he joined the Department of Electrical and Computer Engineering, University of Tehran, where he is currently an Associate Professor. He also has been a Visiting Professor at the Electrical and Computer Department, University of Waterloo, Waterloo, ON, Canada, and Intelwaves Technologies Chief Technical Officer, since November 2004. His current research interests include MIMO and smart antenna systems and the applications of coding and diversity techniques to wireless communications. He is the coauthor of a book entitled *Coded Modulation Techniques for Fading Channel* (New York: Kluwer Academic, 1994).

Kiarash Narimani received the Ph.D. degree in electrical and computer engineering from the University of Waterloo, Waterloo, Ontario, Canada in 2007.

He is currently Senior Software Engineer at Intelwaves Technologies Ltd., Waterloo, ON, Canada. His research interests include wireless systems, coding techniques, information security, digital right management, and computer architecture.

Mircea Hossu was born in Bucharest, Romania, in 1977. He received the B.A.Sc. and M.A.Sc. degrees in electrical engineering from the University of Waterloo, Waterloo, ON, Canada, in 2001 and 2007 respectively.

He has held hardware designer positions at Intelwaves, Pixstream/Cisco Systems, Sensors and Software, and Nortel Networks. Currently he is a Freelance Hardware and Software Contractor based in Canada and Romania.

Hamid Bolandhemmat has a background in aerospace engineering, flight dynamics and a control major, from Sharif University of Technology, Iran. He is currently working toward the Ph.D. degree at the University of Waterloo, Waterloo, ON, Canada.

He is concurrently a Control Engineer at Intelwaves Technologies Ltd., Waterloo. His research interests are estimation, control and navigation.

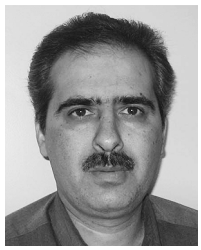

Gholamreza Rafi received the B.Sc. degree from Isfahan University of Technology, Isfahan, Iran, 1991 and the M.Sc. and Ph.D. degrees from Amirkabir University of Technology (Tehran Polytechnic), Tehran, Iran, in 1997 and 2000, respectively, all in electrical engineering.

He was an Assistant Professor in the Electrical Engineering Department, University of Zanjan, Zanjan, Iran, from 2000 to 2001, and collaborated with the Iran Telecommunication Centre (ITRC) as a Research Scientist. He was a Postdoctoral Fellow in the ECE Department, University of Manitoba, Winnipeg, Canada, from 2001 to 2004 and was with Intelwaves Technology from 2005 until 2008. He is currently with the Electrical and Computer Department, University of Waterloo, Waterloo, ON, Canada, as a Senior Research Scientist and Antenna Laboratory Manager. His research activities are integration of RF circuit with antenna and applied electromagnetics

Safieddin Safavi-Naeini was born in Gachsaran, Iran, in 1951. He received B.Sc. degree in electrical engineering from the University of Tehran, Tehran, Iran, in 1974 and the M.Sc. and Ph.D. degrees in electrical engineering from the University of Illinois at Urbana-Champaign, in 1975 and 1979, respectively.

He joined the Electrical Engineering Department, University of Tehran, as an Assistant Professor in 1980 and become an Associate Professor in 1988. In 2002, he joined the E&CE Department, University of Waterloo, as a full Professor. His research interests and activities include numerical electromagnetics applied to RF/microwave/millimeter wave systems and circuits, antenna and propagation, wireless communication systems, very high speed digital circuits, and optical communication systems. He has been scientific and technical consultant to a number of national and international telecommunication industrial and research organizations since 1980.